





Nonlinear defect theory of thermal relaxation in complex multimoded systems

Emily Kabat ¹, Alba Y. Ramos ^{1,2,3,*}, Lucas J. Fernández-Alcázar ^{1,2,3} and Tsampikos Kottos ¹

¹Wave Transport in Complex Systems Lab, Department of Physics, Wesleyan University, Middletown, Connecticut 06459, USA

²Institute for Modeling and Innovative Technology, IMIT (CONICET - UNNE), Corrientes W3404AAS, Argentina

³Physics Department, Natural and Exact Science Faculty, National University of the Northeast, Corrientes W3404AAS, Argentina



(Received 11 April 2024; accepted 25 June 2024; published 26 July 2024)

We show that a single nonlinear defect can thermalize an initial excitation towards a Rayleigh-Jeans (RJ) state in complex multimoded systems. The thermalization can be hindered by disorder-induced localization phenomena, which drive the system into a metastable RJ state. It can differ dramatically from the thermal RJ and it involves only a (quasi)isolated set of prethermal modes whose density can be predicted using a renormalization group theory. Importantly, we establish a connection between the modal relaxation rates that dictate the dynamics towards (quasi)equilibrium and the Thouless conductance. This connection allows us to derive the whole modal relaxation rate distribution. Our results are relevant to photonics, optomechanics, and cold atoms.

DOI: [10.1103/PhysRevResearch.6.033114](https://doi.org/10.1103/PhysRevResearch.6.033114)

I. INTRODUCTION

The complex dynamics of many-body/many-mode systems in response to nonlinear interactions is emerging as fundamental to many different fields ranging from physics, chemistry, and quantum information sciences to biology and sociology [1–6]. Approaches that focus on the microscopic behavior of such systems fail to provide actionable descriptions. The one theory that has proven powerful is statistical mechanics and thermodynamics [7–9]. However, many branches of science and technology have yet to adapt a theory of thermodynamics and statistical mechanics suitable to their field. For instance, the photonics community has only recently begun to develop a thermodynamic theory of beam dynamics in nonlinear multimode photonic platforms (NMPPs) such as multicore/multimode optical fibers [10–14]. In these systems, even at moderate injected powers, nonlinear interactions dominate the beam evolution by introducing mode-mixing effects that redistribute the initial power across individual modes [15–19]. Such complex many-mode configurations are most naturally described by a statistical framework.

In the few years since its conception [10], optical thermodynamics (OT) has proven extremely successful at predicting the modal power distribution of NMPPs. The key tenet of the OT theory, the prediction of a thermal optical state taking the form of a Rayleigh-Jeans (RJ) power distribution, has been observed by various experimental groups using different NMPPs [16,20–23]. Such developments hold promise for a variety of technological applications including the design

of efficient cooling schemes for high-power sources (lasers) [16,24–27] or new fiber structures for medical imaging (endoscopy) [28–30] and fiber optic communications [31,32]. Another field that could benefit from developments in OT and photonics is the area of cold atoms [33,34].

All current efforts are focusing on the analysis of thermalization in systems with spatially distributed nonlinearities, overlooking the fundamental scenario of one nonlinear impurity. To start with, is one nonlinear defect capable of causing thermalization? If so, what are the timescales of such a process? How might the complexity/disorder of the underlying linear structure impact the power redistribution of an initial excitation?

Here, we demonstrate that even one nonlinear defect can lead to thermalization of an initial beam excitation towards RJ. The simplicity of the setting allows us to derive analytical expressions for the whole statistics of the modal relaxation rates that dictate the dynamics towards (quasi)equilibrium. The theoretical results are confirmed via detailed numerics with one-dimensional and quasi-one-dimensional multimoded systems with one nonlinear defect. Our analysis establishes analogies between the relaxation rates and the Thouless conductance describing transport in mesoscopic structures. In chaotic/ergodic systems [35–37], the distribution is Porter-Thomas, indicating a cohesive relaxation behavior of all modes and the suppression of large relaxation rates. As Anderson localization effects due to disorder become dominant [38–40], the distribution shifts towards a log normal with a group of fast relaxing modes separated from the rest. These modes play a prominent role by enforcing a two-stage thermalization process and bear analogies to the prethermalized modes occurring in quantum many-body localized systems [41]. They first converge to a metastable RJ state that differs, sometimes dramatically, from the thermal state. In the case of spatial symmetries, the mode separation can be more extreme: for example, in 1D periodic lattices we observe a bimodal distribution of fast and slow (even vanishing) relaxation rates.

*Contact author: albayramos@exa.unne.edu.ar

Published by the American Physical Society under the terms of the [Creative Commons Attribution 4.0 International](https://creativecommons.org/licenses/by/4.0/) license. Further distribution of this work must maintain attribution to the author(s) and the published article's title, journal citation, and DOI.

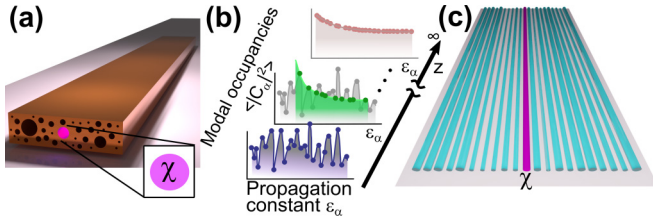


FIG. 1. Schematics of (a) a quasi-one-dimensional multimode waveguide with transverse random long-range coupling (J_{nl}) and (c) a 1D array of waveguides with disordered propagation constants. The magenta core/waveguide indicates the position m of the nonlinear defect with strength χ . (b) An initial preparation of mode occupancies $\langle |C_\alpha(z=0)|^2 \rangle$ (blue) evolves toward a prethermal state (green) characterized by a prethermal RJ distribution composed of only a fraction of the modes. At very long propagation distances ($z \rightarrow \infty$), the system thermalizes to a RJ distribution (red) incorporating all modes.

Using ideas from renormalization group theory [42] (RGT) we describe the density of prethermal modes \mathcal{N} by a first-order nonlinear differential equation that takes the simple universal form

$$\frac{\partial \mathcal{N}}{\partial \ln N} = \beta(\mathcal{N}), \quad (1)$$

where N is the total number of modes of the system. The above equation implies that the logarithmic derivative is a function of \mathcal{N} alone.

The structure of the paper is as follows. In the next section, we present the theoretical models that describe one-dimensional and quasi-one-dimensional multimoded structures with one nonlinear defect. Our analysis reveals the mechanism by which such a single defect drives the thermalization as the disorder increases. Section III examines the emergence of prethermal modes and the formation of metastable states. Section IV develops an one-parameter scaling theory for the density of these prethermal modes. Finally, Sec. V analyzes the modal relaxation rates towards both a metastable and a final RJ equilibrium distribution. We find the whole statistics of relaxation rates and make connections with concepts from mesoscopic theory of transport and specifically the distribution of Thouless conductance. Our conclusions and outlook are discussed in the last section, VI.

II. THEORETICAL FRAMEWORK

We consider beam propagation in one-dimensional (1D) and quasi-1D photonic networks [40,43,44], Figs. 1(a) and 1(c). The beam dynamics is described by a coupled mode theory

$$i \frac{d\psi_l}{dz} = \sum_n J_{ln} \psi_n + \chi \delta_{lm} |\psi_l|^2 \psi_l, \quad l = 1, \dots, N, \quad (2)$$

where ψ_l describes the complex field amplitude at the l th core/waveguide, and the timelike variable z is the paraxial propagation distance. The last term encodes a Kerr nonlinearity, with χ being the strength of the nonlinear defect at site m .

The connectivity matrix J determines the geometry of the system, where nondiagonal elements J_{ln} describe the coupling between sites l and n , and the $J_{l,l}$'s correspond to the propagation constants associated with each core/waveguide. The setup in Fig. 1(a) can be modeled by a banded random matrix (BRM) [45–48] whose elements J_{ln} are given by a normal Gaussian distribution with mean zero $\langle J_{nl} \rangle = 0$ and variance $\langle J_{nl}^2 \rangle = \frac{N+1}{b(2N-b+1)}$ for $|n-l| < b$ and $J_{nl} = 0$ for $|n-l| \geq b$. This normalization guarantees that the Hamiltonian (internal energy) associated with Eq. (2) is extensive. The parameter b defines the long-range coupling and can induce Anderson localization of the linear supermodes with localization length $\ell_\infty \sim b^2$. The limit $b \rightarrow N$ corresponds to the GOE matrices used in Ref. [11] for the analysis of thermalization of wave chaotic systems via spatially extended nonlinearities. We also consider the 1D case of Fig. 1(c), modeled by a nearest-neighbor (NN) connectivity matrix with $J_{l,l\pm 1} = 1$ and random $J_{ll} \in [-\frac{W}{2}, \frac{W}{2}]$ given by a box distribution. The localization length [49,50] of the supermodes is given by $\ell_\infty \approx 24(4 - \varepsilon^2)/W^2$.

We represent Eq. (2) using the supermode basis $f_\alpha(l)$, where l refers to the site index and α the mode index. Then, $\psi_l(z) = \sum_\alpha e^{-i\varepsilon_\alpha z} C_\alpha(z) f_\alpha(l)$, and Eq. (2) reads

$$i \frac{dC_\alpha}{dz} = \chi \sum_{\beta\gamma\delta} Q_{\alpha\beta\gamma\delta} C_\beta^* C_\gamma C_\delta e^{i(\varepsilon_\alpha + \varepsilon_\beta - \varepsilon_\gamma - \varepsilon_\delta)z}, \quad (3)$$

where ε_α is the α eigenvalue. The right-hand side (RHS) represents the mode-mode interactions, where

$$Q_{\alpha\beta\gamma\delta} = f_\alpha^*(m) f_\beta^*(m) f_\gamma(m) f_\delta(m) \quad (4)$$

determines the strength of the four-wave mode mixing introduced by the nonlinear defect.

In general, the rate of power exchange between various modes is determined by two processes: the degree of phase matching ($\varepsilon_\alpha + \varepsilon_\beta - \varepsilon_\gamma - \varepsilon_\delta \approx 0$) and the strength of the mode-mode interaction. When $Q_{\alpha\beta\gamma\delta}$ is structureless, as in chaotic wave systems where the amplitudes $f_\alpha(m)$ are comparable across all α eigenmodes, the phase matching mechanism is the only means by which our systems can achieve thermalization. When the degree of mode overlap $f_\alpha(m)$ at the nonlinear defect m is α dependent, $Q_{\alpha\beta\gamma\delta}$ acquires a structure that becomes relevant for the analysis of the modal power distribution $|C_\alpha(t)|^2$. Specifically, modes that have a high amplitude at the nonlinear site have the potential to be involved in many significant four-wave mode interactions. Conversely, modes with small amplitudes are excluded from all four-wave mode interactions. Thus we see the emergence of two groups of modes: interacting ones and noninteracting ones. These two groups act as (quasi)isolated systems with constant internal energy and power.

III. PRETHERMALIZED MODES AND METASTABLE RJ

While standard analysis of the power redistribution in NMPPs involves the numerical integration of many coupled differential equations [see Eqs. (2) and (3)], the recent development of optical thermodynamics (OT) offers an elegant alternative [10–12]. This framework posits a thermal equilibrium without addressing questions about the

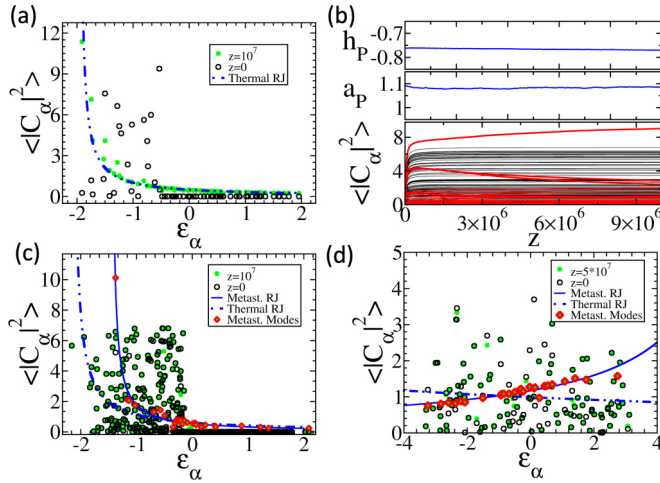


FIG. 2. (a) Initial (black circles) and final (green circles) modal occupations for a BRM with $b = N = 64$. Due to supermode ergodicity, the entire system reaches a RJ thermal state (dashed blue line) with $(T, \mu) = (1.0, -2.0)$. (b) Evolution of energy density $h_P \equiv \mathcal{H}_P/N_P$ (top), optical power density $a_P \equiv \mathcal{A}_P/N_P$ (middle), and modal occupation $\langle |C_\alpha(z)|^2 \rangle$ (bottom). The prethermal modes (red) display a long-lived stability after reaching the prethermal RJ state. (c) BRM setting, displaying a metastable RJ state (solid blue line) with $(T_P, \mu_P) = (0.8, -1.5)$ that differs dramatically from the final RJ state (dashed blue line) with $(T, \mu) = (1.3, -2.2)$. Prethermal modes are highlighted in red diamonds. (d) NN equivalent of (c), with $(T_P, \mu_P) = (-8.8, 7.5)$ and $(T, \mu) = (24.9, -25.2)$. In (b)–(c) $N = 512$, $b = 3$, and $m = 256$. In (d), $N = 128$, $W = 4$, and $m = 70$. In all cases $\chi = 0.05$.

thermalization process. It identifies intrinsic variables T, μ that are optical thermodynamic forces analogous to chemical potential and temperature in traditional statistical mechanics. Both are uniquely determined by the two constants of motion of Eq. (3): total power $\mathcal{A} = \sum_\alpha |C_\alpha|^2$ and total internal energy $\mathcal{H} \approx \mathcal{H}_{\text{Linear}} = \sum_\alpha \epsilon_\alpha |C_\alpha|^2$ (assuming weak nonlinearities) [51]. The thermal RJ distribution of modal power takes the form $\langle |C_\alpha|^2 \rangle = n_\alpha = \frac{T}{\epsilon_\alpha - \mu}$ where $\langle \cdot \rangle$ indicates thermal averaging.

In Fig. 2(a) we examine a typical scenario of structureless $Q_{\alpha\beta\gamma\delta}$ that displays a predicted RJ thermal distribution (dashed blue line). The main figure reports the final $|C_\alpha|^2$ s (green circles) associated with a random initial preparation (black circles), demonstrating that, even though $Q_{\alpha\beta\gamma\delta} \sim 1/N^2$, a single nonlinear defect is able to thermalize the whole array of size N .

Next, we consider the case of structured $Q_{\alpha\beta\gamma\delta}$, which we achieve by inducing Anderson localization of the supermodes f_α . This separates the modes into two distinct groups: those with high amplitude at the position of the nonlinear defect can interact with each other, while the rest are isolated. Due to the exponential localization, only modes that are centered in the proximity $\sim \ell_\infty$ of the nonlinear defect will belong to the first group. Combinations exclusively involving such modes will provide large $Q_{\alpha\beta\gamma\delta}$'s that will overpower the phase-matching mechanism. In practice, we have established a cutoff amplitude $|f_\alpha^{\text{cutoff}}(m)|^2 \propto \langle \sum_l |f_\alpha(l)|^4 \rangle_\alpha$ to identify these high-amplitude interacting modes. We have

corroborated the selection of these modes by monitoring their modal power evolution.

This set of N_P prethermal modes maintains (quasi)constant internal energy \mathcal{H}_P and power \mathcal{A}_P for an exponentially long time [see Fig. 2(b)]. This is suggestive of a thermodynamic analysis pertaining to a long-lived metastable state. Applying the OT methodology to this subset we can extract from $\mathcal{H}_P, \mathcal{A}_P$ the corresponding T_P, μ_P defining a metastable RJ that dictates the power distribution among the prethermal modes. Importantly, as shown in Figs. 2(c) and 2(d) the metastable RJ (solid blue line) might differ drastically from the final thermal RJ (dashed blue line). The open black circles and the solid green circles represent the initial and postevolution power distributions, respectively, evaluated via a direct numerical integration of Eq. (2). The prethermal modes that form the metastable RJ distribution are highlighted with red diamonds. We underline once more the longevity of these metastable states, which renders them more practically relevant than the thermal RJ distribution. This can be seen in Fig. 2(b) where the temporal evolution of the power occupations is shown for the longest time that we have computationally achieved. The formation of a metastable RJ is unique to cases of structured $Q_{\alpha\beta\gamma\delta}$, as systems displaying structureless $Q_{\alpha\beta\gamma\delta}$ thermalize directly to the thermal RJ without undergoing an intermediate metastable configuration.

IV. ONE-PARAMETER SCALING AND β -FUNCTION FORMALISM

We are now equipped to formulate a one-parameter scaling theory that describes the number of prethermal modes N_P . The underlying ansatz is that, although the metastable RJ is determined by numerous system parameters (disorder configuration, connectivity, position of the nonlinear defect, N, \mathcal{H} , and \mathcal{A}), the number of prethermal modes is a simple function of the scaling variable $\ell_{\text{rel}} \equiv \ell_\infty/N$. In other words, we postulate the existence of a universal function

$$\mathcal{N} \equiv \frac{N_P}{N_{\text{ref}}} = \Phi(\ell_{\text{rel}}) \approx \begin{cases} \ell_{\text{rel}} & \text{for } \ell_{\text{rel}} < 0.1 \\ 1 & \text{for } \ell_{\text{rel}} > 1 \end{cases}, \quad (5)$$

where $N_{\text{ref}} \propto N$ is the number of prethermal modes associated with an underlying structureless (ergodic) system, which acts as a reference system. For example, for BRM modeling, the reference ensemble is the full RMT $b = N$, where all modes are prethermal, i.e., $N_{\text{ref}} = N$ and therefore $\mathcal{N} = N_P/N$ is the density of prethermal modes [52]. We have numerically tested the validity of Eq. (5) by integrating Eq. (2) using both BRM and NN connectivity matrices J_{ln} . In the case of BRMs (NNs) various system sizes $64 \leq N \leq 2048$ ($64 \leq N \leq 256$) and bandwidths $3 \leq b \leq 64$ (disorder strengths $0.01 \leq W \leq 4$) have been used. The numerical data shown in Fig. 3 confirms the scaling ansatz Eq. (5), encapsulating the transition from completely thermalizing systems ($\mathcal{N} \rightarrow 1$) to systems that support metastable states ($\mathcal{N} < 1$). Specifically, when the supermodes are extended over the whole system ($\ell_{\text{rel}} > 1$), they all have a non-negligible amplitude at the nonlinear defect, and the entire system thermalizes. Conversely, when the localization length is smaller than the system size, ($\ell_{\text{rel}} < 1$), the number of modes that interact with the nonlinear defect is $\sim \ell_\infty$, and thus, the prethermal modes will have a density

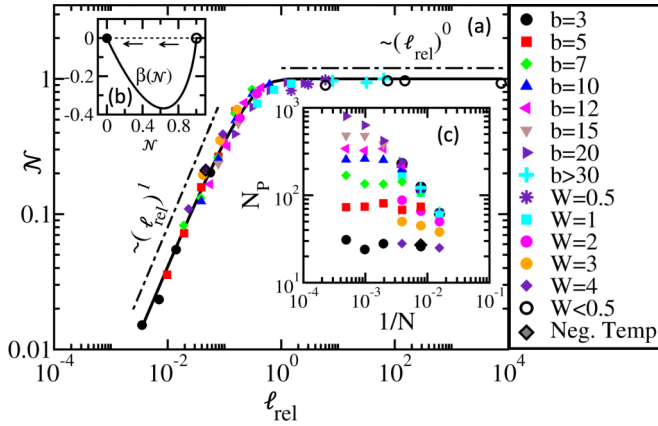


FIG. 3. (a) Prethermal mode density (\mathcal{N}), described by a one-parameter function $\mathcal{N}(\ell_{\text{rel}}) = 1 - e^{-5.4\ell_{\text{rel}}}$ that only depends on the relative localization length (ℓ_{rel}). Data from both NN and BRM systems are shown. Dot-dashed lines indicate the ℓ_{rel}^1 and ℓ_{rel}^0 behaviors. (b) β -function associated with Eq. (1), featuring two fixed points at $\mathcal{N} = 1$ (unstable) and $\mathcal{N} = 0$ (stable). (c) Unscaled data showing the number of prethermal modes as a function of N^{-1} .

$\mathcal{N} \sim \ell_{\text{rel}}$. A law valid in all regimes is $\Phi(\ell_{\text{rel}}) = 1 - e^{-C\ell_{\text{rel}}}$ where $C = 5.4$ is the best fitting parameter, see Fig. 3(a).

Following ideas from renormalization group theory (RGT) we recast Eq. (5) into an equivalent form given by Eq. (1). This formulation highlights the fact that the density of prethermal modes is a solution of a (nonlinear) first-order differential equation. The resulting β function takes the form $\beta(\mathcal{N}) = (1 - \mathcal{N}) \cdot \ln(1 - \mathcal{N})$, which is always negative in the domain of definition $\mathcal{N} \in [0, 1]$ [see Fig. 3(b)]. Moreover, it is a continuous function since it describes how the density of the prethermal modes evolves as a function of system size N . Notice that, unlike the typical β functions in RGT, our β function is nonmonotonic in \mathcal{N} and features two fixed points, a stable one at $\mathcal{N} = 0$ and an unstable one at $\mathcal{N} = 1$. This is physically consistent with the fact that increasing the system size N will decrease the fraction of prethermal modes \mathcal{N} .

V. RELAXATION DYNAMICS

The dynamics towards the metastable and/or the thermal RJ state are described via a kinetic equation (KE) approach. The latter is derived from Eq. (2) under the following assumptions [18,53,55]: (i) weak nonlinearities that ensure the appropriateness of the linear supermode basis; (ii) phase randomization of the field amplitudes; (iii) localization lengths l_∞ , which are much larger than the lattice spacing such that many linear supermodes are mixed with one another; (iv) finally, the kinetic approach requires the system to be away from the condensate regime where the normal modes of the nonlinear equation Eq. (2) (linearized around the nonuniform condensate), differ from the linear eigenmodes. The resulting kinetic equation takes the form:

$$\frac{dI_\alpha}{dt} = 4\pi\chi^2 \sum_{\beta\gamma\delta} |Q_{\alpha\beta\gamma\delta}|^2 I_\alpha I_\beta I_\gamma I_\delta \left(\frac{1}{I_\alpha} + \frac{1}{I_\beta} - \frac{1}{I_\gamma} - \frac{1}{I_\delta} \right) \times \delta(\varepsilon_\alpha + \varepsilon_\beta - \varepsilon_\gamma - \varepsilon_\delta), \quad (6)$$

where $I_\alpha = I_\alpha(t)$ describes the optical power occupying the linear supermode α at time t and the summation \sum' excludes the secular terms.

The analysis of the modal relaxation rates requires a linearization of Eq. (6). Specifically, we considered small variations of the modal powers around their RJ equilibrium value, i.e., $I_\alpha \rightarrow n_\alpha + \delta I_\alpha$. Substitution of the perturbed modal powers in Eq. (6) and neglecting the off-diagonal contributions in the relaxation process (see detailed description for the derivation in Refs. [54,55]) we arrive at the following equation for the modal relaxation rates Γ_α of the α th mode towards its equilibrium value $n_\alpha = T/(\varepsilon_\alpha - \mu)$,

$$\Gamma_\alpha = \frac{4\pi\chi^2}{n_\alpha} \sum_{\beta\gamma\delta}' |Q_{\alpha\beta\gamma\delta}|^2 n_\beta n_\gamma n_\delta \delta(\varepsilon_\alpha + \varepsilon_\beta - \varepsilon_\gamma - \varepsilon_\delta). \quad (7)$$

The numerical evaluation of Eq. (7) utilized matrices of size $N = 512, 1024$. Numerically, we implement the δ function in the rate equation using a tolerance $\Delta_{\text{tol}} = 0.01$. This value has been chosen to guarantee that the calculations converge for all disorder strengths under consideration. Additionally, we have confined our analysis to a small frequency window such that we only consider α modes at the center of the band. For the statistical processing, we have used a sufficient number of disorder realizations to ensure that the total number of relaxation rates exceeded 35000 data.

The form of $Q_{\alpha\beta\gamma\delta}$ specific to the current problem of one nonlinear defect [see Eq. (4)] allows us to further reduce Eq. (7) to

$$\Gamma_\alpha \propto \chi^2 F_\alpha(T, \mu) \times |f_\alpha(m)|^2, \quad (8)$$

where $F_\alpha(T, \mu)$ incorporates the various mode-mixing terms appearing in the triple sum in Eq. (7). When analyzing the distribution of relaxation rates $\mathcal{P}(\Gamma)$ towards the thermal RJ, we assume that the α -supermode intensity at the position of the defect $|f_\alpha(m)|^2$ is the dominant statistical term in Eq. (8). (For a validation of this assumption, see the Appendix.) From the theoretical perspective, therefore, the statistical analysis of Γ_α 's collapse to the analysis of the supermode intensities at the defect site. Below we test the theoretical predictions that rely on this assumption with a direct comparison of the relaxation rates evaluated numerically via Eq. (7).

A. Statistics of relaxation rates in chaotic systems

We begin with the distribution of relaxation rates in case of ergodic systems. In linear wave chaotic structures, the distribution of supermode amplitudes is derived using Berry's random superposition hypothesis of plane waves [35,36]. Then, the probability density of intensities follows the so-called Porter-Thomas (PT) distribution $\mathcal{P}(y = N|f_\alpha|^2) = (1/\sqrt{2\pi y})e^{-y/2}$. From these considerations, we conclude that $\mathcal{P}(\tilde{\Gamma} = N\Gamma)$ follows the distribution

$$\mathcal{P}(\tilde{\Gamma} = N\Gamma) \approx \left(\frac{1}{\sqrt{2\pi c\tilde{\Gamma}}} \right) e^{-\tilde{\Gamma}/2c}, \quad (9)$$

which resembles the standard Porter-Thomas statistics differing only by the additional factor of $1/c$ in the exponent. This factor arises from the proportionality factor $\Gamma_\alpha/(\chi^2|f_\alpha(m)|^2)$ appearing in Eq. (7). Furthermore, our numerical

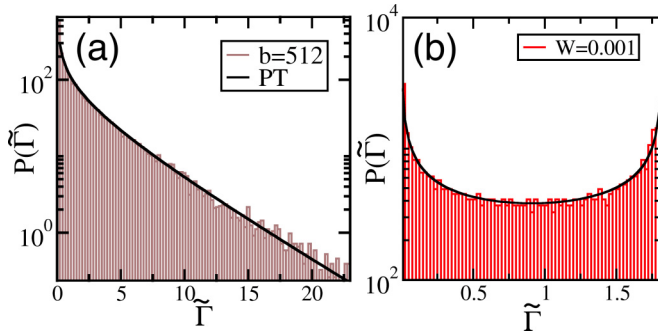


FIG. 4. (a) The distribution of relaxation rates \mathcal{P} towards the thermal RJ of ballistic/chaotic systems. The PT distribution shown is for $\mathcal{P}(\tilde{\Gamma}) \sim 1/\sqrt{\tilde{\Gamma}}\exp(-\tilde{\Gamma}/2c)$, with $c \approx 2.5$. (b) The distribution of a 1D lattice with $W = 0.001$, which exhibits a bimodal behavior resulting from the symmetry of the system.

analysis on this proportionality factor indicates that $c \approx 2.5$ (see Appendix).

In Fig. 4(a) we report our results of the numerical evaluation of Eq. (4) together with the PT prediction Eq. (9). The observed agreement corroborates our original assumption that the fluctuations of F_α are not relevant for the statistics of relaxation rates. The above distribution guarantees a well-defined mean relaxation rate $\langle \tilde{\Gamma} \rangle \propto \mathcal{O}(1)$, which reflects the fact as the number of modes N (equivalent to volume in standard thermodynamics) increases the relaxation rates $\Gamma \rightarrow 0$.

Peculiar behaviors might arise in cases where symmetries interfere with the underlying wave chaotic nature of a linear system. For example, in the limiting case $W \rightarrow 0$ of 1D translational-invariant lattices, $f_\alpha(m) \sim N^{-1/2} \sin(k_\alpha m)$. Assuming uniformly distributed wave vectors $k_\alpha \in [-\pi, \pi]$, we get

$$\mathcal{P}(\tilde{\Gamma} \equiv \Gamma N) \sim [\tilde{\Gamma}(1 - \tilde{\Gamma}/2)]^{-1/2}, \quad (10)$$

which is a bimodal distribution. The above distribution indicates that there are two groups of fast- and slow- (or non)thermalizing modes. Indeed, in this case, one can distinguish between modes that have a nodal point at the position of the nonlinear defect, and therefore do not thermalize, and modes that have an antinodal point and therefore thermalize easily. The numerical data resulting from the exact evaluation of Eq. (4) are shown in Fig. 4(b) together with the theoretical prediction Eq. (10).

B. Statistics of relaxation rates in localized systems

Next, we analyze the scenario where localization dominates the relaxation process. In this case, we deduce from Eq. (8) that $\Gamma_\alpha \sim |f_\alpha(m)|^2 \sim \exp(-2|x_\alpha - m|/l_\infty + \eta_{x_\alpha})$, where x_α represents the localization center of the α th mode. The stochastic variable η_{x_α} introduces Gaussian noise with zero mean and variance $(\Delta\eta_{x_\alpha})^2 = |x_\alpha - m|/l_\infty$ that describes random fluctuations around the mean intensity profile [56]. Considering only the smallest relaxation rates, corresponding to modes α for which $|x_\alpha - m| \sim N$, this Gaussian noise dominates the statistics. Consequently, the statistics for

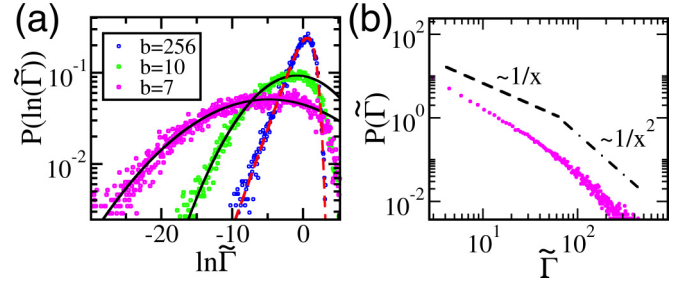


FIG. 5. The distribution of relaxation rates \mathcal{P} towards the thermal RJ of a disordered system in the localized regime. We see that as the system becomes more localized, the distribution stretches out to incorporate more slow-relaxing modes. (a) Demonstrates the log-normal distribution arising in localized systems. Colored circles represent data from the evaluation of relaxation rates, and the black lines are the theoretical predictions for localized systems [Eq. (11)]. For $b = 256$, the system is entering the extended regime, so the corresponding red dashed line is a PT distribution [Eq. (9)]. (b) shows the $1/\tilde{\Gamma}$ and $1/\tilde{\Gamma}^2$ behaviors of the fast-relaxing modes of the most localized system ($b = 7$).

this group of modes is given by

$$\begin{aligned} \mathcal{P}(\tilde{\Gamma}) &= \mathcal{P}(\eta_{x_\alpha}) \frac{d\eta_{x_\alpha}}{d\tilde{\Gamma}} \sim \exp\left(\frac{-\ell_\infty \eta_{x_\alpha}^2}{2|x_\alpha - m|}\right) \frac{d\eta_{x_\alpha}}{d\tilde{\Gamma}} \\ &\sim \exp\left(\frac{-\ell_\infty [\ln^2(\tilde{\Gamma}/\tilde{\Gamma}_0) - 2 \ln(\tilde{\Gamma}/\tilde{\Gamma}_0) \ln(\tilde{\Gamma}_0)]}{2N}\right) \tilde{\Gamma}^{-1}, \end{aligned}$$

where $\ln(\tilde{\Gamma}_0) = -N/l_\infty$. Since this distribution applies in the limit of small $\tilde{\Gamma}$, we can neglect the $\ln(\tilde{\Gamma}/\tilde{\Gamma}_0)$ term, such that we recover a log-normal distribution.

$$\mathcal{P}(\tilde{\Gamma}) \sim \exp((-\ell_\infty/2N) \ln^2(\tilde{\Gamma}/\tilde{\Gamma}_0)) \tilde{\Gamma}^{-1}. \quad (11)$$

Such a distribution is typical for the conductance statistics of localized chains reflecting the normal distribution of the inverse localization length around its mean value in the localized regime [49]. These predictions have been tested using both disordered 1D NN and quasi-1D BRM matrix models. Our numerical results are nicely described by the above theoretical predictions, see Fig. 5(a).

Next, we consider the group of modes with localization centers closer to the defect site, such that x_α is uniformly distributed in the proximity $\sim \ell_\infty$ of the defect site. In this case, the Gaussian noise in the intensity profile can be neglected and the relaxation rates can be approximated as $\Gamma_\alpha \sim |f_\alpha(m)|^2 \sim \exp(-2|x_\alpha - m|/l_\infty)$ where the localization centers x_α are considered to be uniformly distributed across a localization domain $\sim l_\infty$ around the nonlinear defect. Thus,

$$P(\tilde{\Gamma}) \sim \tilde{\Gamma}^{-1}, \quad (12)$$

which nicely describes an intermediate range of Γ rates, see Fig. 5(b).

For the description of the modes with the fastest relaxation rates (i.e., extreme right part of the distribution), we employ a heuristic (classical) argument. We associate each mode with a classical particle that explores the space ballistically. When this particle reaches the nonlinear defect it scatters to other modes—a process that leads to their relaxation. In

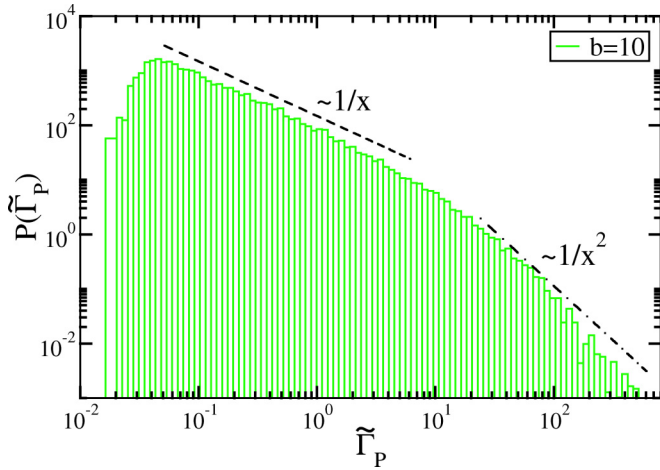


FIG. 6. We report $\mathcal{P}(\tilde{\Gamma}_P)$ of the (quasi)isolated set of prethermal modes. The lines are the corresponding theoretical predictions (see text). We also see the expected cutoff at $\tilde{\Gamma} \sim 10^{-2}$.

this respect, the number of particles (modes) that relax by time $\tau_R \sim 1/\Gamma$ is proportional to the number of particles that reside within a distance $L_R \sim \tau_R$ away from the defect. The above consideration assumes a ballistic spreading of the modes, which is expected to describe the dynamics of short timescales where localization effects due to disorder are not yet dominant. Furthermore, since each mode is localized to a specific site, we associate the number of particles (modes) that reach the relaxation center (nonlinear defect) with L_R . In other words $L_R \sim \int_{\Gamma}^{\infty} P(\Gamma') d\Gamma' \sim 1/\Gamma$ whose derivative $P(\Gamma) = -dL_R(\Gamma)/d\Gamma$ determines the probability density of relaxation rates. We have

$$\mathcal{P}(\tilde{\Gamma}) \sim \tilde{\Gamma}^{-2}. \quad (13)$$

This heuristic argument captures nicely the behavior of the numerical data, see Fig. 5(b). Of course, the above argumentation provides only a qualitative rationale and a more rigorous derivation is desirable.

Similar arguments apply to the relaxation rates Γ_P of the prethermal modes towards their metastable RJ. When evaluating the relaxation process towards the metastable state, the summation involved in $F_{\alpha}(T, \mu)$ is restricted to the N_P (quasi)isolated prethermal modes. Then, repeating the same steps as above, we conclude that the distribution $\mathcal{P}(\tilde{\Gamma}_P) \sim 1/\tilde{\Gamma}_P$, with the fastest relaxation rates again following the distribution $\mathcal{P}(\tilde{\Gamma}_P) \sim 1/\tilde{\Gamma}_P^2$. We also note that the restriction of the summation to the N_P prethermal modes gives a lower bound for F_{α} , which in turn bounds Γ_{α} . The numerical evaluation of the relaxation rates is shown in Fig. 6 and nicely confirms the above considerations.

Let us finally point out that the rescaled form of the relaxation rates $\tilde{\Gamma}$ that naturally appears in our analysis is reminiscent of the Thouless conductance defined as $g_T = \gamma/\Delta$ where $\Delta \sim 1/N$ is the mean level spacing and γ is the linewidth of resonant modes. Like the Thouless conductance captures the disordered/chaotic nature of mesoscopic transport, our $\tilde{\Gamma}$ probes the underlying complexity of the linear systems in the thermalization process and reflects the transition from a ballistic to a localized behavior.

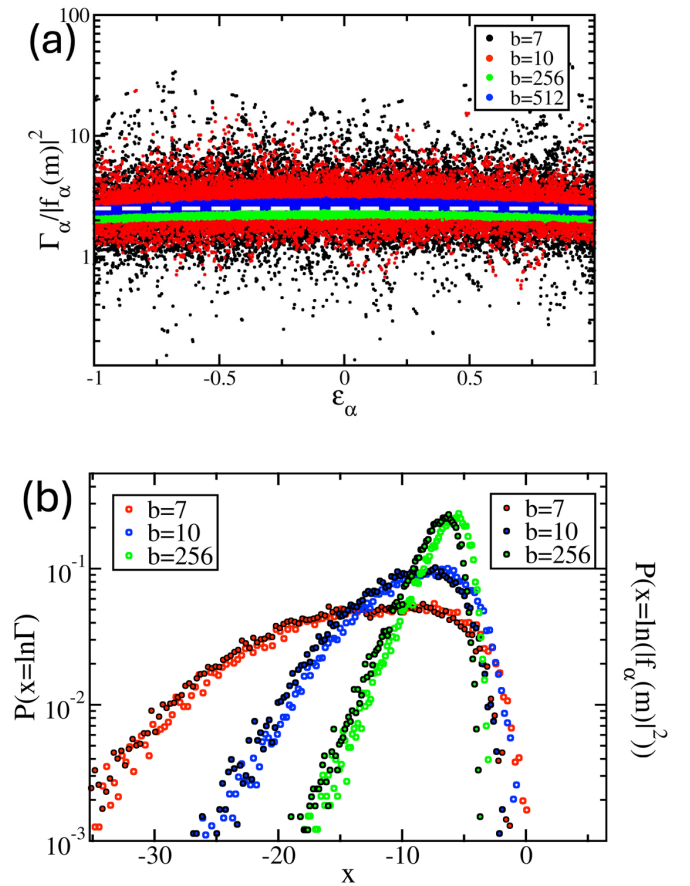


FIG. 7. (a) The ratio of Γ_{α} to $|f_{\alpha}(m)|^2$ for each mode α of a BRM system of size $N = 512$. The ratio is approximately constant, and varies only slightly on the selected mode. The dashed white line indicates the average value of $\Gamma_{\alpha}/|f_{\alpha}(m)|^2 \approx 2.5$. This confirms that the statistics of Γ_{α} are indeed determined by the statistics of $|f_{\alpha}(m)|^2$. (b) The distributions of Γ_{α} (colored circles) and $|f_{\alpha}(m)|^2$ (colored circles with black border) for a BRM system of size $N = 512$ with a variety of different bandwidths, showing that the two variables do in fact have the same statistics. For both (a) and (b), similar results were found for NN systems.

VI. CONCLUSIONS

We have analyzed the thermalization process of a beam propagating in complex nonlinear multimoded systems. We found that even a single nonlinear defect is capable of inducing thermalization described by an RJ thermal state. When Anderson localization effects are dominant, the mode-mode interactions acquire a nonuniform structure. This enforces the formation of metastable RJ states whose optical temperature and chemical potential can be dramatically different from the ones defining the thermal RJ state. The density of prethermal modes is determined by a universal β function, which describes the system without recourse to its microscopic details.

The simplicity of our model also allows us to evaluate the relaxation rates of the modes towards their (pre)thermal state. The key element in the analysis is the connection between relaxation rates and wave-function statistics. The latter is well studied in the framework of mesoscopic physics for chaotic/disordered systems. Building on this connection, we

have been able to analyze the whole statistics of relaxation rates, which was found to resemble closely the statistics of resonances and Thouless conductance of mesoscopic systems.

The above connection and the potential use of a nonlinear defect as a probe for Anderson localization (AL), is not at all trivial. Indeed, for the study of AL one needs to select states at a given energy ε . However, in the thermalization problem the four-mode interaction mixes modes with different energies, so that even if the initial preparation selects a fixed energy, the subsequent evolution will create excitations in other energies. Further investigations along these lines are necessary in order to establish this criterion as a probe for AL.

ACKNOWLEDGMENTS

We acknowledge support from the MPS Simons Collaboration via Grant No. 733698. A.Y.R. and L.J.F.-A. acknowledge partial support from CONICET and MINCyT Grant No. CONVE-2023-10189190 - FFLASH and the hospitality of

Wesleyan University. This work used computational resources from CCAD-UNC, which is part of SNCAD-MinCyT, and the high-performance computing cluster of IMIT (CONICET-UNNE), Argentina. We acknowledge useful discussions with Professor B. Shapiro.

APPENDIX: DEPENDENCE OF $\mathcal{P}(\tilde{\Gamma})$ ON $|f_\alpha(m)|^2$

We have stated that $\Gamma_\alpha \propto F_\alpha \times |f_\alpha(m)|^2$, and proceeded assuming that $|f_\alpha(m)|^2$ is the dominant statistical term. Here, we numerically demonstrate the validity of this assumption. Figure 7(a) shows the ratio $\Gamma_\alpha/|f_\alpha(m)|^2$ versus ε_α for various values of the bandwidth b and clearly demonstrates that the ratio is a constant independent of α . The white line indicates the center of the distribution at a value ≈ 2.5 , which is used in the derivation of the Porter-Thomas distribution. In Fig. 7(b), we observe that the close match between the probability distribution functions of Γ_α and the ones associated with $|f_\alpha(m)|^2$, further confirming the proportionality between these two statistics.

-
- [1] A. T. Winfree, *The Geometry of Biological Time* (Springer, Berlin, 1980).
- [2] A. C. Oates, L. G. Morelli, and S. Ares, Patterning embryos with oscillations: Structure, function and dynamics of the vertebrate segmentation clock, *Development* **139**, 625 (2012).
- [3] L. He, X. Wang, H. L. Tang, and D. J. Montell, Tissue elongation requires oscillating contractions of a basal actomyosin network, *Nature Cell Biol.* **12**, 1133 (2010).
- [4] E. D. Herzog, Neurons and networks in daily rhythms, *Nature Rev. Neurosci.* **8**, 790 (2007).
- [5] D. H. Geschwind and P. Levitt, Autism spectrum disorders: developmental disconnection syndromes, *Current Opin. Neurobiol.* **17**, 103 (2007).
- [6] R. Nandkishore and D. A. Huse, Many-body localization and thermalization in quantum statistical mechanics, *Annu. Rev. Condens. Matter Phys.* **6**, 15 (2015).
- [7] F. Reif, *Fundamentals of Statistical and Thermal Physics* (McGraw-Hill, New York, 1965).
- [8] H. B. Callen, *Thermodynamics and an Introduction to Thermostatistics* (John Wiley & Sons, New York, 1985).
- [9] L. E. Reichl, *A Modern Course in Statistical Physics*, 2nd ed. (Wiley, New York, 1998).
- [10] F. Wu, A. Hassan, and D. Christodoulides, Thermodynamic theory of highly multimoded nonlinear optical system, *Nature Photon.* **13**, 776 (2019).
- [11] A. Ramos, L. Fernandez-Alcazar, T. Kottos, and B. Shapiro, Optical phase transitions in photonic networks: A spin-system formulation, *Phys. Rev. X* **10**, 031024 (2020).
- [12] K. G. Makris, F. O. Wu, P. S. Jung, and D. N. Christodoulides, Statistical mechanics of weakly nonlinear optical multimode gases, *Opt. Lett.* **45**, 1651 (2020).
- [13] Q. Zhong, F. O. Wu, A. U. Hassan, R. El-Ganainy, and D. N. Christodoulides, Universality of light thermalization in multimoded nonlinear optical systems, *Nat. Commun.* **14**, 370 (2023).
- [14] F. O. Wu, P. S. Jung, M. Parto, M. Khajavikhan, and D. N. Christodoulides, Entropic thermodynamics of nonlinear photonic chain networks, *Commun. Phys.* **3**, 216 (2020).
- [15] A. Fusaro, J. Garnier, K. Krupa, G. Millot, and A. Picozzi, Dramatic acceleration of wave condensation mediated by disorder in multimode fibers, *Phys. Rev. Lett.* **122**, 123902 (2019).
- [16] L. G. Wright, F. O. Wu, D. N. Christodoulides, and F. W. Wise, Physics of highly multimode nonlinear optical systems, *Nat. Phys.* **18**, 1018 (2022).
- [17] A. Picozzi, J. Garnier, T. Hansson, P. Suret, S. Randoux, G. Millot, and D. N. Christodoulides, Optical wave turbulence: Towards a unified nonequilibrium thermodynamic formulation of statistical nonlinear optics, *Phys. Rep.* **542**, 1 (2014).
- [18] S. Nazarenko, *Wave Turbulence*, Lecture Notes in Physics, Vol. 825 (Springer-Verlag, Berlin, 2011).
- [19] S. Nazarenko, A. Soffer, and M.-B. Tran, On the wave turbulence theory for the nonlinear Schrödinger equation with random potentials, *Entropy* **21**, 823 (2019).
- [20] K. Baudin, A. Fusaro, K. Krupa, J. Garnier, S. Rica, G. Millot, and A. Picozzi, Classical Rayleigh-Jeans condensation of light waves: observation and thermodynamic characterization, *Phys. Rev. Lett.* **125**, 244101 (2020).
- [21] H. Pourbeyram, P. Sidorenko, F. O. Wu, N. Bender, L. Wright, D. N. Christodoulides, and F. Wise, Direct observations of thermalization to a Rayleigh-Jeans distribution in multimode optical fibres, *Nat. Phys.* **18**, 685 (2022).
- [22] A. L. Marques-Muniz, F. O. Wu, P. S. Jung, M. Khajavikhan, D. N. Christodoulides, and U. Peschel, Observation of photon-photon thermodynamic processes under negative optical temperature conditions, *Science* **379**, 1019 (2023).
- [23] K. Baudin, J. Garnier, A. Fusaro, N. Berti, C. Michel, K. Krupa, G. Millot, and A. Picozzi, Observation of light thermalization to negative-temperature Rayleigh-Jeans equilibrium states in multimode optical fibers, *Phys. Rev. Lett.* **130**, 063801 (2023).

- [24] L. G. Wright, D. N. Christodoulides, and F. W. Wise, Spatiotemporal mode-locking in multimode fiber lasers, *Science* **358**, 94 (2017).
- [25] A. Kurnosov, L. J. Fernández-Alcázar, A. Y. Ramos, B. Shapiro, and T. Kottos, Optical kinetic theory of nonlinear multi-mode photonic networks, *Phys. Rev. Lett.* **132**, 193802 (2024).
- [26] M. Lian, Y.-J. Chen, Y. Geng, Y. Chen, and J.-T. Lü, Violation of the Wiedemann-Franz law in coupled thermal and power transport of optical waveguide arrays, *arXiv:2307.16529*.
- [27] S. Iubini, S. Lepri, and A. Politi, Nonequilibrium discrete nonlinear Schrödinger equation, *Phys. Rev. E* **86**, 011108 (2012).
- [28] C. Barsi, W. Wan, and J. W. Fleischer, Imaging through nonlinear media via digital holography, *Nat. Photon.* **3**, 211 (2009).
- [29] M. Plöschner, T. Tyc, and T. Cizmár, Seeing through chaos in multimode fibres, *Nature Photon.* **9**, 529 (2015).
- [30] A. P. Mosk, A. Lagendijk, G. Lerosey, and M. Fink, Controlling waves in space and time for imaging and focusing in complex media, *Nature Photon.* **6**, 283 (2012).
- [31] D. J. Richardson, J. M. Fini, and L. E. Nelson, Space division multiplexing in optical fibers, *Nature Photon.* **7**, 354 (2013).
- [32] K.-P. Ho and J. M. Kahn, *Mode Coupling and Its Impact on Spatially Multiplexed Systems, Optical Fiber Telecommunications VIB* (Elsevier, New York, 2013).
- [33] M. Abuzarli, N. Cherroret, T. Bienaimé, and Q. Glorieux, Nonequilibrium prethermal states in a two-dimensional photon fluid, *Phys. Rev. Lett.* **129**, 100602 (2022).
- [34] T. Scoquart, D. Delande, and N. Cherroret, Dynamical emergence of a Kosterlitz-Thouless transition in a disordered Bose gas following a quench, *Phys. Rev. A* **106**, L021301 (2022).
- [35] K. Efetov, *Supersymmetry in Disorder and Chaos* (Cambridge University Press, Cambridge, 1996).
- [36] H.-J. Stöckmann, *Quantum Chaos: An Introduction* (Cambridge University Press, Cambridge, 1999).
- [37] F. Haake, *Quantum Signatures of Chaos* (Springer, Berlin, 2001).
- [38] P. W. Anderson, Absence of diffusion in certain random lattices, *Phys. Rev.* **109**, 1492 (1958).
- [39] M. Segev, Y. Silberberg, and D. N. Christodoulides, Anderson localization of light, *Nature Photon.* **7**, 197 (2013).
- [40] A. Mafi and J. Ballato, Review of a decade of research on disordered Anderson localizing optical fibers, *Front. Phys.* **9**, 736774 (2021).
- [41] M. Ueda, Quantum equilibration, thermalization and prethermalization in ultracold atoms, *Nat. Rev. Phys.* **2**, 669 (2020).
- [42] E. Abrahams, P. W. Anderson, D. C. Licciardello, and T. V. Ramakrishnan, Scaling theory of localization: Absence of quantum diffusion in two dimensions, *Phys. Rev. Lett.* **42**, 673 (1979).
- [43] B. Abaie and A. Mafi, Scaling analysis of transverse Anderson localization in a disordered optical waveguide, *Phys. Rev. B* **94**, 064201 (2016).
- [44] Y. Lahini, A. Avidan, F. Pozzi, M. Sorel, R. Morandotti, D. N. Christodoulides, and Y. Silberberg, Anderson localization and nonlinearity in one-dimensional disordered photonic lattices, *Phys. Rev. Lett.* **100**, 013906 (2008).
- [45] F. M. Izrailev, Simple models of quantum chaos: Spectrum and eigenfunctions, *Phys. Rep.* **196**, 299 (1990).
- [46] G. Casati, L. Molinari, and F. Izrailev, Scaling properties of band random matrices, *Phys. Rev. Lett.* **64**, 1851 (1990).
- [47] Y. V. Fyodorov and A. D. Mirlin, Scaling properties of localization in random band matrices: A σ -model approach, *Phys. Rev. Lett.* **67**, 2405 (1991).
- [48] C. W. J. Beenakker, Random-matrix theory of quantum transport, *Rev. Mod. Phys.* **69**, 731 (1997).
- [49] E. N. Economou, *Green's Functions in Quantum Physics* (Springer, Berlin, 1979).
- [50] B. Kramer and A. MacKinnon, Localization: Theory and experiment, *Rep. Prog. Phys.* **56**, 1469 (1993).
- [51] K. Ø. Rasmussen, T. Cretegny, P. G. Kevrekidis, and N. Grønbech-Jensen, Statistical mechanics of a discrete nonlinear system, *Phys. Rev. Lett.* **84**, 3740 (2000).
- [52] In cases of networks with symmetries, N_{ref} might be slightly smaller than the size of the system reflecting the underlying symmetries that prohibit the ergodicity of the supermodes. For example, NN networks with $W = 0$ have supermodes whose nodal points may coincide with the position of the nonlinear defect, and thus, $Q_{\alpha\beta\gamma\delta} = 0$. These modes would not participate in the thermalization process (even in the limit of infinite time). In such cases, one needs to assume the limiting value of N_{ref} as $W \rightarrow 0$. One can envision possibilities to exploit this scenario as protection against information melting.
- [53] V. E. Zakharov, V. S. L'vov, and G. E. Falkovich, *Kolmogorov Spectra of Turbulence I: Wave Turbulence* (Springer-Verlag, Berlin, 1992).
- [54] A. Y. Ramos, C. Shi, L. J. Fernández-Alcázar, D. N. Christodoulides, and T. Kottos, Theory of localization-hindered thermalization in nonlinear multimode photonics, *Commun. Physics* **6**, 189 (2023).
- [55] C. Shi, T. Kottos, and B. Shapiro, Controlling optical beam thermalization via band-gap engineering, *Phys. Rev. Res.* **3**, 033219 (2021).
- [56] F. M. Izrailev, T. Kottos, A. Politi, and G. P. Tsironis, Evolution of wave packets in quasi-one-dimensional and one-dimensional random media: Diffusion versus localization, *Phys. Rev. E* **55**, 4951 (1997).